Applied Surface Science, Volume 552, 30 June 2021, Article number 149489
DOI:10.1016/j.apsusc.2021.149489

Accepted in Applied surface Science on 3rd March 2021

Origins of ductile plasticity in a polycrystalline gallium arsenide during scratching: MD simulation study

Pengfei Fan[1], Saurav Goel[2,3,4,5*], Xichun Luo[1*], Yongda Yan[6], Yanquan Geng[6] and Yang He[6]

[1] Centre for Precision Manufacturing, DMEM, University of Strathclyde, UK

[2] School of Engineering, London South Bank University, 103 Borough Road, London SE1 0AA, UK

[3] School of Aerospace, Transport and Manufacturing, Cranfield University, Bedfordshire, MK43 0AL, UK

[4] Department of Mechanical Engineering, Shiv Nadar University, Gautam Budh Nagar, 201314, India

[5] Department of Mechanical Engineering, Indian Institute of Technology, Guwahati, 781039, India

[6] Center for Precision Engineering, Harbin Institute of Technology, Harbin, P. R. China

*Corresponding email: GoeLs@Lsbu.ac.uk and xichun.luo@strath.ac.uk

Abstract

This paper used molecular dynamics simulation to obtain an improved understanding of the ductile plasticity in polycrystalline gallium arsenide (GaAs) during its nanoscratching. Velocity-controlled nanoscratching tests were performed with a diamond tool to study the friction-induced deformation behaviour of polycrystalline GaAs. Cutting temperature, sub-surface damage depth, cutting stresses, the evolution

of dislocations and the subsequent microstructural changes were extracted from the simulation. The simulated MD data indicated that the deformation of polycrystalline GaAs is accompanied by dislocation nucleation in the grain boundary leading to the initiation of plastic deformation. Furthermore, a dual slip mechanism was observed as an important factor driving plasticity in poly GaAs in sharp contrast to a single GaAs. The magnitude of cutting forces and the extent of sub-surface damage were both observed to reduce with an increase in the scratch velocity whereas the cutting temperature scaled with the cutting velocity. As for the depth of the scratch, an increase in its magnitude increased the cutting forces, temperature and damage-depth. A phenomenon of fluctuation from wave crests to wave troughs in the cutting forces was observed only during the cutting of polycrystalline GaAs and not during the cutting of single-crystal GaAs.

Keywords: Polycrystalline gallium arsenide; MD simulation; Grain boundary; Dislocation nucleation

1 Introduction

Gallium arsenide (GaAs) has emerged as a favourable choice as a III-V direct bandgap semiconductor due to its applications in 5G communication devices [1]. GaAs (which resides in a Zinc-blende structure) possesses superior properties to silicon, for instance, GaAs has a higher saturated electron velocity and higher electron mobility, allowing GaAs transistors to function swiftly at frequencies over 250 GHz. Owing to their wider energy bandgap, GaAs devices are relatively insensitive to overheating which makes

46 them less noisy while operating at higher frequencies in electronic circuits and that is
47 where they outbid silicon devices. GaAs can be grown as a single crystal using methods
48 such as the vertical gradient freeze method, the Bridgman-Stockbarger technique, or
49 the Liquid encapsulated Czochralski growth process. Parallel to this, the use of
50 polycrystalline GaAs as thin films is quite popular. Films of GaAs can be grown by
51 chemical vapour deposition (by annealing an amorphously grown film), or by using
52 molecular beam epitaxy (MBE). The processing cost of polycrystalline GaAs is lower
53 than the processing cost of single crystal GaAs [2] and this allows polycrystalline GaAs
54 to find wider applications in the field of solar cells [3][4], imaging detectors [5],
55 microwave and optoelectronic devices [6].
56 Prior work suggests that poly and single crystals of silicon [7][8] and silicon carbide
57 [9] showed differences in the incipient plasticity and material removal mechanism,
58 although the fundamental reasons behind these differences were not immediately clear.
59 The microstructure of material (such as grain boundaries and defects) also influences
60 the Schottky barrier height. There are knowledge gaps like these that prompted the
61 authors to investigate the mechanical deformation of polycrystalline GaAs using
62 molecular dynamics (MD) simulation. As such, recent advances made in the
63 computation hardware now offer the possibility [10] to use MD simulations as an
64 advanced digital nano manufacturing tool. The remaining sections of the paper discuss
65 the scratch forces, sub-surface damage, peak cutting temperature, cutting stresses in a
66 polycrystalline substrate benchmarked against a single crystal GaAs substrate.
67

2 MD simulation methodology

2.1 MD simulation model

An orthogonal MD simulation nanoscratching model for cutting a polycrystalline GaAs was developed using the Voronoi site-rotation algorithm (see figure 1 and figure 2(a)). The diamond scratching tool was modelled with a negative rake angle of -25° and a clearance angle of 10°. The polycrystalline GaAs workpiece was built by employing the Atomsk software [11] using the Voronoi algorithm [12][13]. The Voronoi site-rotation method generates a polycrystalline structure by joining the normals of the line of random discrete points at the crystal boundary and containing the growing random oriented crystal seeds. As shown in Fig. 2(b), the polycrystalline GaAs workpiece was divided into three regions of atoms i.e. Newtonian atoms (yellow and red color atoms), thermostat atoms (blue color atoms) and boundary atoms (green color atoms). Prior to cutting, the GaAs workpiece (containing 14 grains) was equilibrated for about 100 ps using the Nose-Hoover method [14] in LAMMPS (Large-scale atomic/molecular massively parallel simulator) [15]. Visualization and analysis were performed using Visual molecular dynamics (VMD) [16] and Open Visualization Tool (OVITO) softwares [17]. The detailed parameters used for the model development are shown in Table 1.

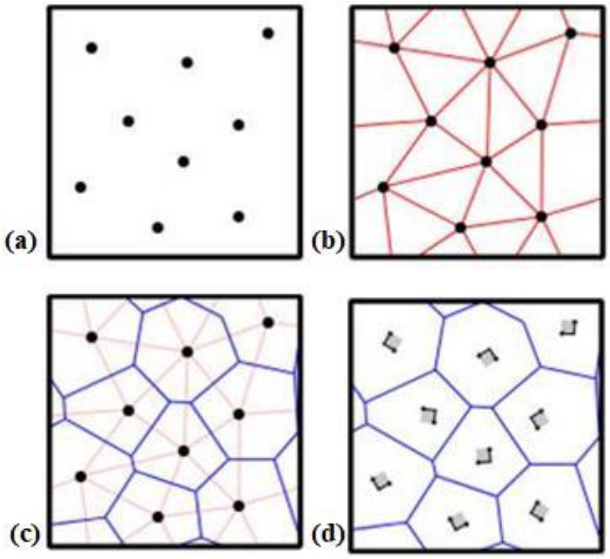

Fig. 1. Voronoi site-rotation illustration showing random points.

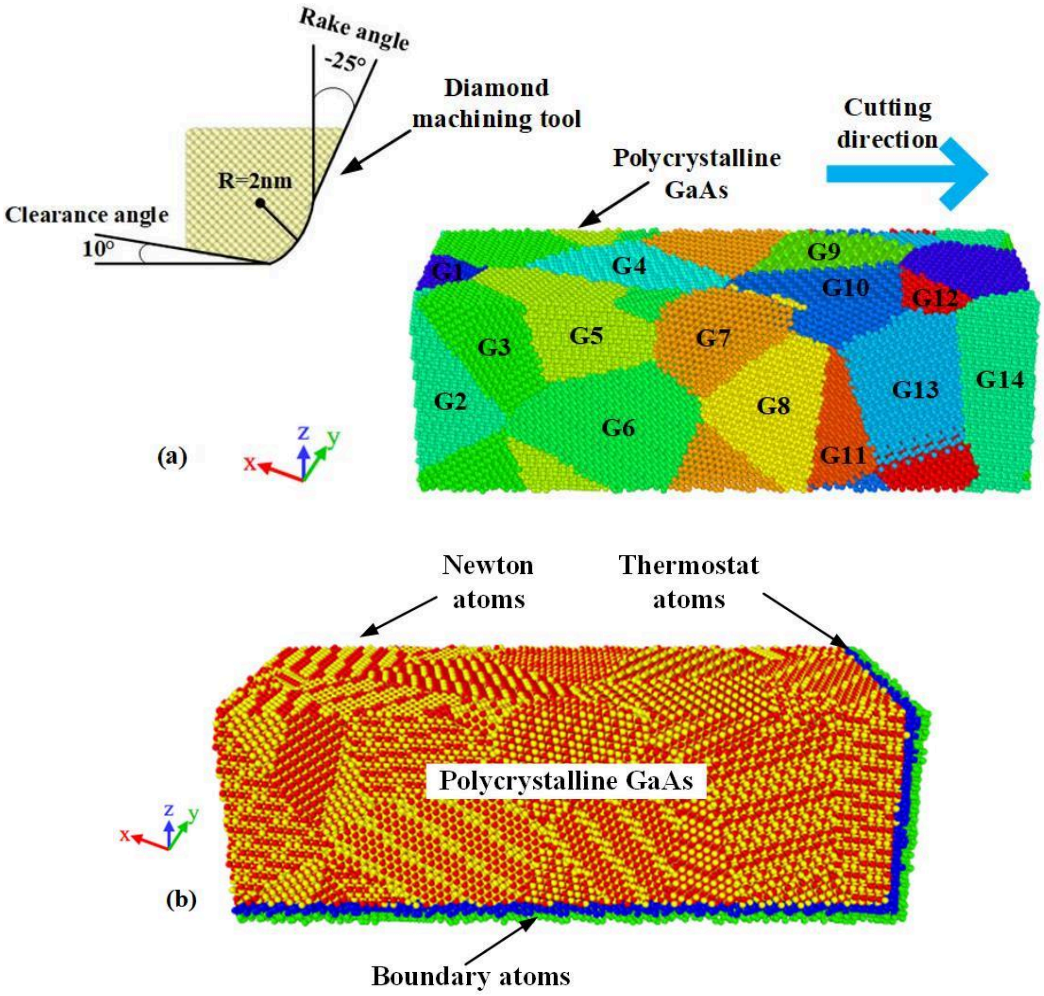

Fig. 2. Nanoscratching model of polycrystalline GaAs showing different grains and tool description.

92 **Table 1**: Simulation parameters used to develop the MD simulation model

GaAs substrate dimensions	30.8 nm × 10.0 nm × 13.4 nm (X, Y and Z direction)
Number of atoms in the polycrystalline GaAs	184285 (total 14 grains)
Scratching tool	Diamond cutting tool (rigid)
Number of atoms in the tool	12085
Tool rake angle	-25°
Tool clearance angle	10°
Tool edge radius	2 nm
Equilibrium lattice constant of GaAs	5.78 Å (Zinc blende lattice structure)
Diamond lattice constant	3.57 Å (Diamond cubic lattice structure)
Width of cut	2.86 nm
Depth of cut	Was varied (0.5 nm, 1 nm and 2 nm)
Scratch velocity	Was varied (100 m/s, 200 m/s and 400 m/s)
Scratching distance	12 nm
Equilibration temperature	300 K
Timestep used for MD calculation	1 fs

93

94 ## *2.2 Selection of potential energy function*

95 The choice of potential function can make a significant difference on the accuracy of
96 MD results. It is important to choose a robust potential especially when it concerns
97 studying aspects of fracture, wear and plasticity of a material. In this investigation, the
98 cutting of GaAs with a diamond tool required describing the interactions between and
99 among three types of atoms namely, Ga, As and C atoms. Due to the unavailability of a
100 single many-body potential parameterized to describe all these atoms, a hybrid scheme
101 was employed here in a hybrid/overlay scheme offered by LAMMPS. For the sake of
102 brevity and avoiding repeated information, the details of the potential function (which
103 is readily available from the respective papers) are not repeated here, but generally

104 speaking, the covalently bonded interactions of C-C and the Ga-Ga, As-As and Ga-As
105 interactions were all described by the analytical bond order potential developed by the
106 research group of Albe et al. [18][19]. As for the cross interactions between the atoms
107 of the diamond tool and the Gallium Arsenide workpiece (Ga-C and As-C), a Ziegler-
108 Biersack-Littmark (ZBL) potential function [20] (pair_style zbl in LAMMPS) was used
109 which simply requires the atomic number and cut off parameters as an input.
110

111 # 3 Results and discussions

112 ## *3.1 Microstructural changes*

113 Taking a test case of cutting depth of 2 nm and scratch velocity of 200 m/s, figure 3
114 shows a simulation output wherein blue color atoms, white color atoms, green color
115 atoms and red color atoms represent the perfect zinc blende (ZB) structure, amorphous
116 (Amp) structure, hexagonal diamond (HD) structure and stacking faults (SF)
117 respectively. The grain boundaries that were analyzed are marked by number 1, 2, and
118 3, respectively.

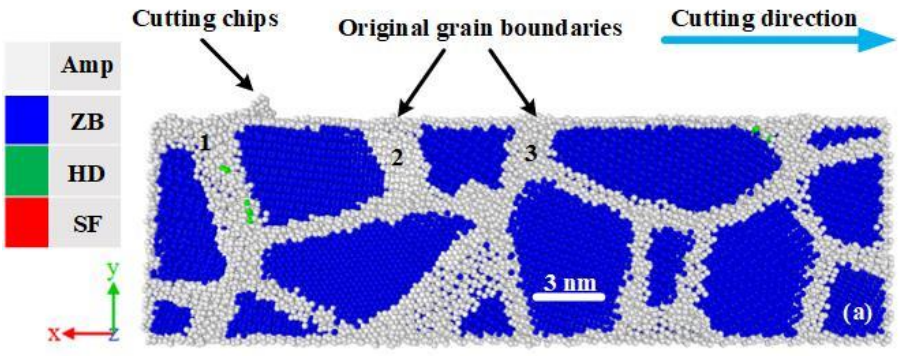

119

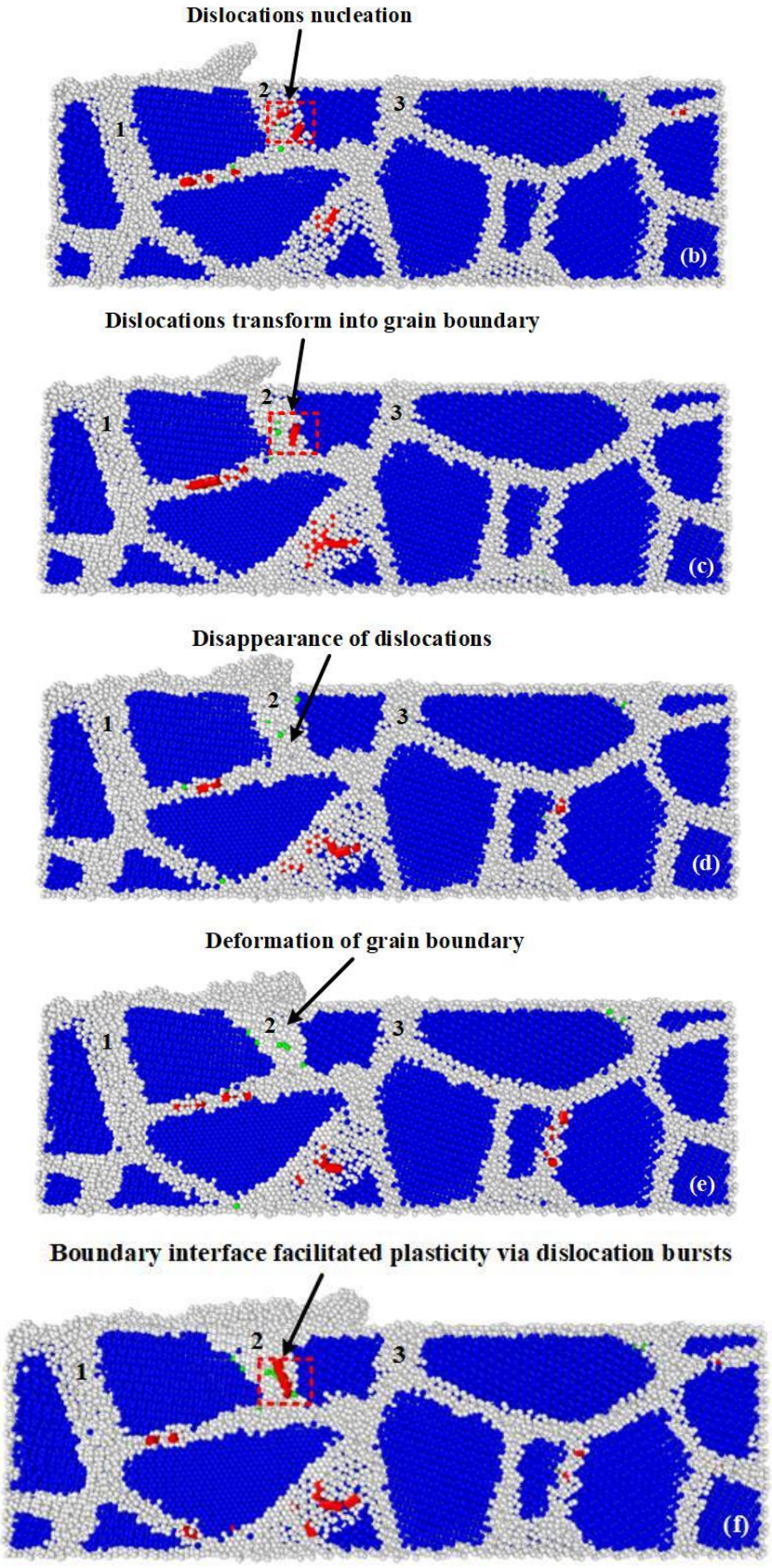

Fig. 3. Cross-sectional image of the polycrystalline GaAs (tool is kept hidden for visualization and cutting is performed at a depth of 2 nm and scratch velocity of 200 m/s). The snapshots are taken at cutting

distances (a) 3 nm, (b) 6 nm, (c) 7 nm, (d) 8 nm, (e) 9 nm and (f) 12 nm. Pictures were processed using OVITO.

As shown in Fig. 3(a), the grain boundaries marked by 1, 2 and 3 were chosen as the sites of analysis for post-processing visualization of the dislocation and stacking fault structures using the second nearest neighbor scheme relying on an extended common neighbor analysis implemented in OVITO [21]. Fig. 3(b) highlights the initiation of the nucleation of dislocations at several places in the grain boundary 2 (GB 2). With subsequent tool travel, i.e. at the cutting distance of 7 nm, a part of the dislocations created at a cutting distance of 6 nm started to transform to grey color atoms and became a part of GB 2. Subsequently, the dislocations within GB 2 disappeared and transformed into a grain boundary marked by grey color atoms at the cutting distance of 8 nm shown in Fig. 3(d). Meanwhile, a small number of green atoms were found present in the grain boundaries. At the cutting distance of 8 nm, the GB 2 widens and became thicker as may be seen in Fig. 3(e). Finally, as shown in Fig. 3(f), a large dislocation burst appeared in the GB 2 at the cutting distance of 12 nm, and a few grey color atoms transformed into red color atoms. The observation reported here remains consistent in all the simulation test cases.

Meanwhile, the evolution of structural changes in polycrystalline GaAs was quantified as a function of cutting velocity at various depths of scratch (see Fig. 4). It must be noted here that the ABOP potential function used in this study does not predict the energy differences between the cubic diamond and hexagonal closed packed diamond and hence the observation of hexagonal diamond in this study is a mere reflection on

the faulted diamond cubic structure [22]. Overall, results in figure 4 show that a higher cutting velocity leads to a reduced degree of structural transformation in the material. Additionally, it was observed that all such microstructural transformations initiate preferentially in the grain boundaries. It implies that grain boundaries are preferred sites of nucleation of dislocations during the scratching of a polycrystalline substrate.

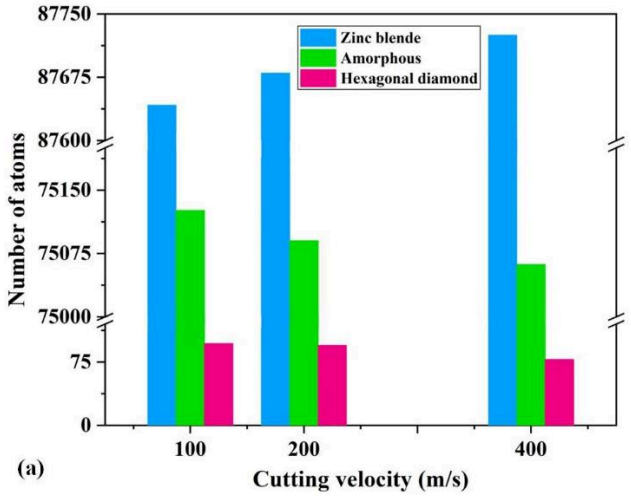

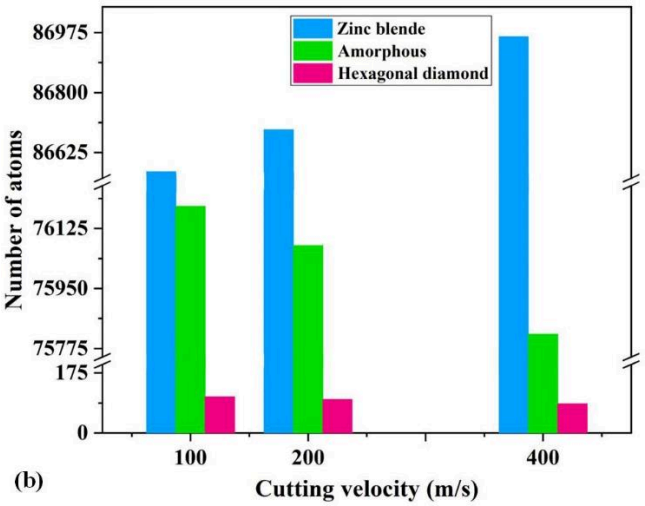

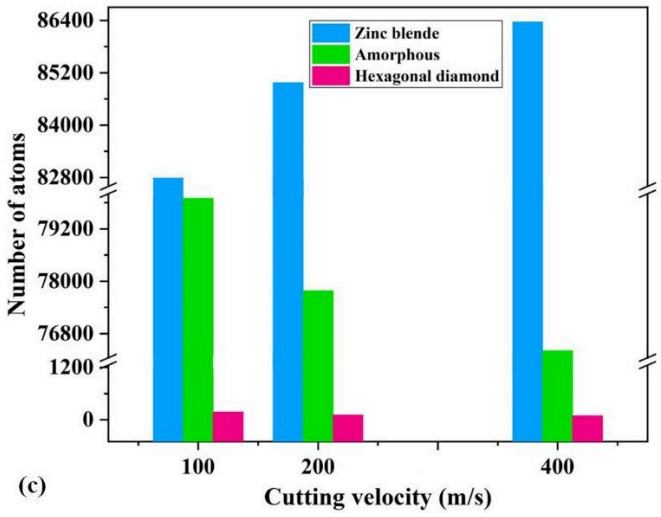

Fig. 4. The evolution of microstructure changes in polycrystalline GaAs during nanoscratching process with various cutting velocities under cutting depth of 0.5 nm (a), 1 nm (b) and 2 nm (c). Note here that the occurrence of the formation of hexagonal diamond is a mere artefact since the potential function used in this study does not distinguish energy differences between cubic and hexagonal phases.

3.2 Analysis of dislocation nucleation

Fig. 5 shows the details of dislocation nucleation. According to the three-dimensional (3D) images, the nucleation of dislocations (marked by red color atoms) occurred in the grain boundaries, which is consistent with the two-dimensional (2D) images shown earlier in Fig. 3. As no dislocations were found inside of the individual grains of polycrystalline GaAs, it indicated that the grain boundaries are softer than the grains and deform swiftly. This phenomenon is in accordance with the recently reported work on polycrystalline silicon carbide material [23]. Additionally, when the diamond tool penetrated the polycrystalline GaAs at 3 nm (see Fig. 5(a)), the two clusters of the dislocations were found in G1-G2 and G5-G6, respectively. Subsequently, the dislocation nucleation diffused through G4-G5 and the right corner of the

polycrystalline GaAs workpiece, as illustrated in Fig. 5(b). In accordance with Fig. 5(c) and Fig. 5(d), the dislocation nucleation kept reappearing when the diamond tool passed through the edge of the grain boundary between G4 and G5. When the diamond tool started to penetrate the grain boundary between G4 and G5, there was no dislocation nucleation in G4-G5 (see figure 5(e)). The dislocation nucleation was distributed across the G5-G6 and G7-G8-G9-G10-G11-G13. Finally, the dislocation nucleation reoccurred in the G4-G5, as showed in Fig. 5(f), while the diamond tool cuts the grain boundary between G4 and G5.

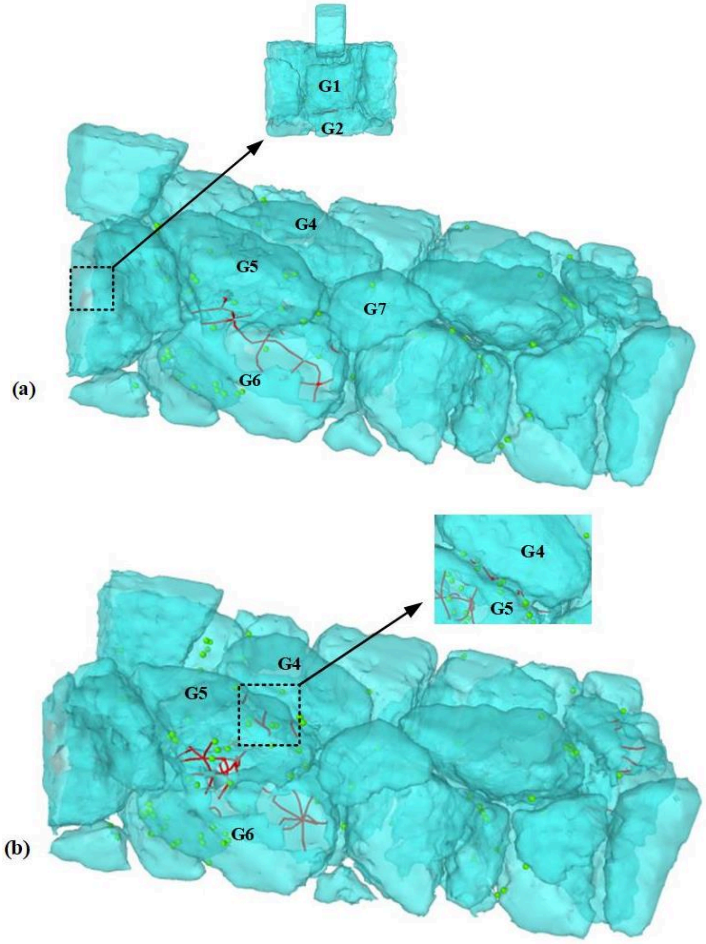

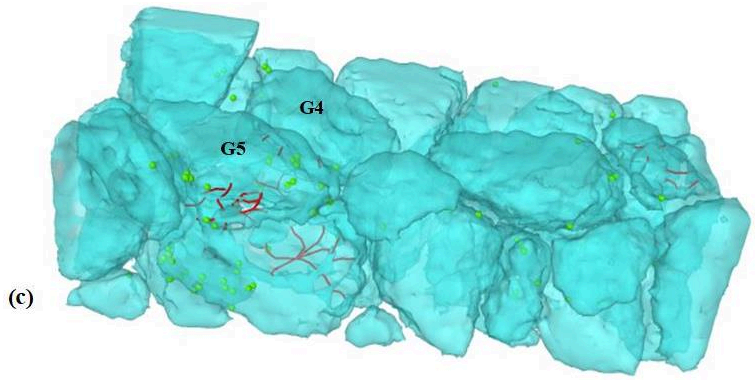

184

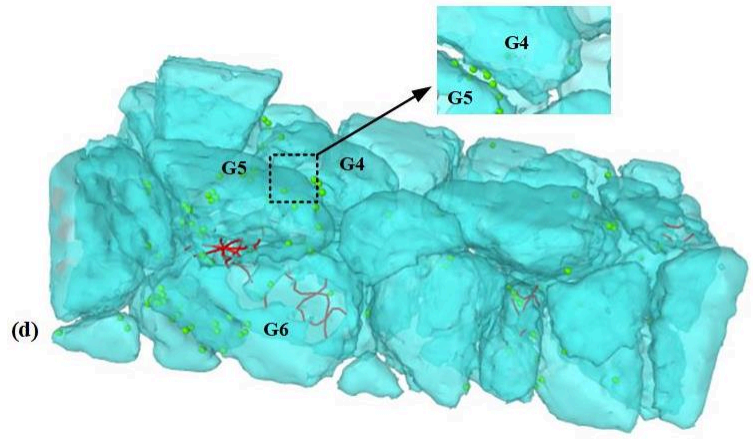

185

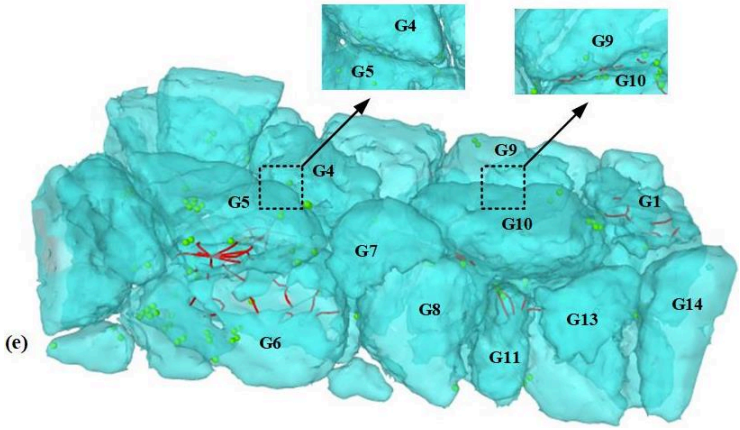

186

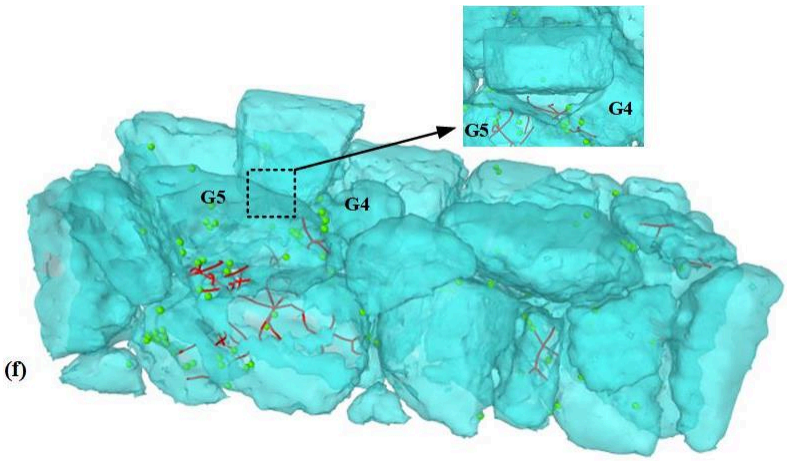

187

Fig. 5. The movement of dislocations in the polycrystalline GaAs at (a) 3 nm (b), 6 nm (c), 7 nm (d), 8 nm (e), 9 nm and (f) 12 nm.

In terms of the quantitative analysis, the number of dislocation segments extracted from the MD data is shown in Fig. 6. It can be seen that the presence of 1/2<110> type dislocations dominated others which was responsible for the incipient plasticity observed in the polycrystalline GaAs. The two other dislocations of type $\frac{1}{6}\langle 112\rangle$ and $\frac{1}{3}\langle 111\rangle$ were also present and were of the same length for the duration of cutting studied here. During the simulation, the dislocation with 1/2[110] Burgers vector was observed to split into two Shockley partials with one having $1/6\,[121]$ Burgers vector and the other having $1/6\,[211]$ Burgers vector. The dissociation reaction can be represented as $1/2\,[110] = 1/6\,[121] + 1/6\,[211]$.

Also, the $1/3\langle 111\rangle$ dislocation with [-110] Burgers vector at 7 nm cutting distance appears to dissociate to a $1/3\langle 111\rangle$ dislocation with [11-2] Burgers vector. This phenomenon suggests the shuffle set dislocations could transit to glide set dislocations under large shear stress caused by the scratching tool [24]. The occurrence of the dual slip mechanisms was seen an important factor driving plasticity in poly GaAs in sharp contrast to a single GaAs.

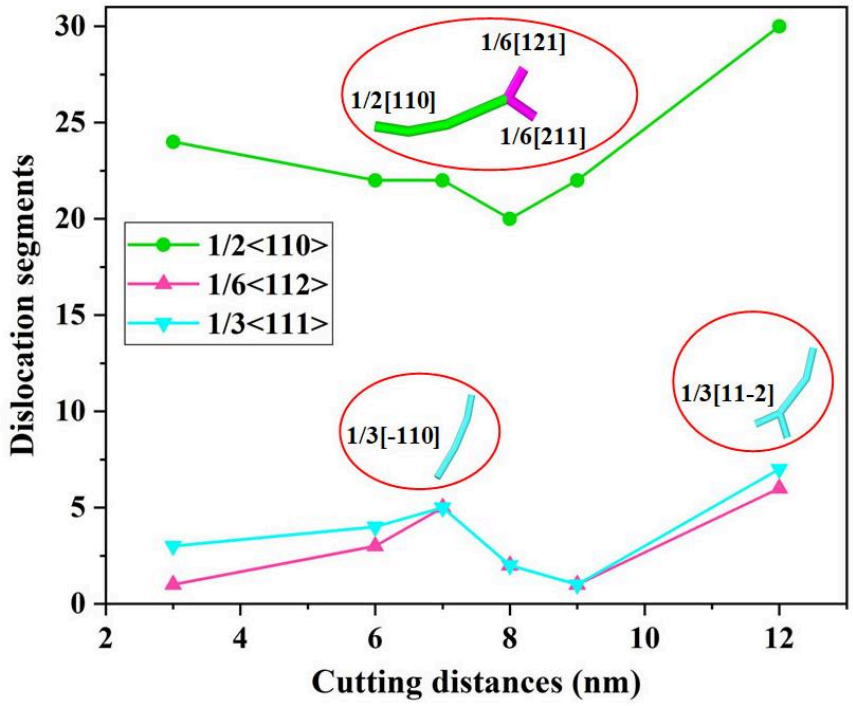

205

206 **Fig. 6.** Variation in the extent of dislocation segments and dislocations images with cutting distance.

207

208 An important physical quantity, dislocation density, was employed to describe the total
209 length of dislocation lines contained in a unit volume of polycrystalline GaAs. The
210 dislocation density was calculated by Eq. (1) [25].

211 $$\rho = \frac{L}{V} \quad (1)$$

212 where the L and V represent the total length of dislocation lines (Å) and volume of
213 workpiece ($Å^3$), respectively. Consequently, the evolution of dislocation density as a
214 functional of scratching distance is illustrated in Fig. 7.

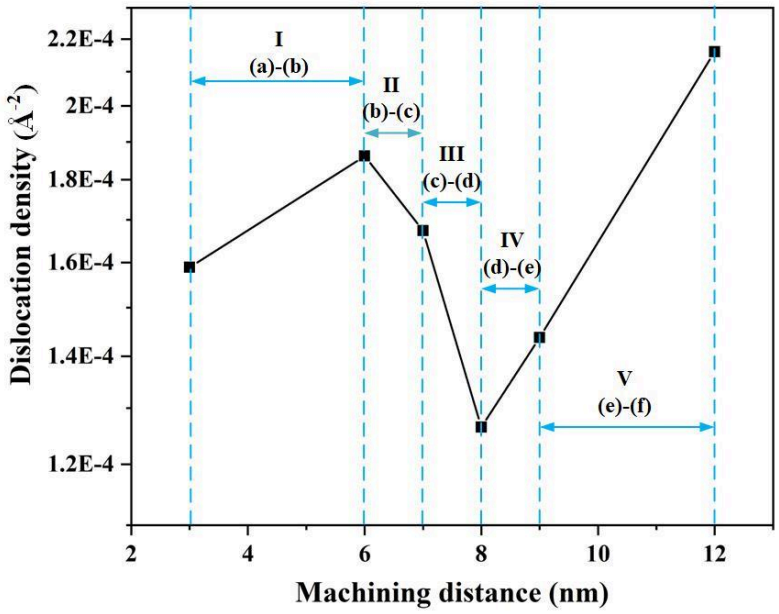

Fig. 7. Evolution of the dislocation density as a function of machining distance.

The dislocation density curve was seen to consist of five stage (I, II, III, IV and V). The dislocation density in the Ist stage was seen to increase which indicated the initiation of dislocation nucleation within the grain boundary. The dislocation density in the IInd and IIIrd stage decreases implied that certain dislocations transform to grain boundaries vis-a-vis disappearing of certain dislocations in a certain grain boundary as shown in Fig. 3 and Fig. 5. The dislocation density of the IV and V stage experienced a significant increase indicating that the diamond tool propagated through the grain boundaries to cause more dislocations and the cycle keeps repeating.

3.3 Differences in the cutting of single crystal and polycrystalline GaAs

During this investigation, additional MD simulations were performed to benchmark the scratch forces namely, the lateral force (F_x) and normal force (F_y) during cutting of polycrystalline GaAs and single crystal GaAs. Fig 8 shows the evolution of the scratch

231 forces obtained from the MD simulations while cutting polycrystalline GaAs and single
232 crystal GaAs substrates. Initially, until the onset of chip formation (unsteady cutting
233 condition), the lateral force (F_x) was seen to be larger than the normal force (F_y) and
234 once the machining achieved a steady-state, then the normal force (F_y) becomes larger
235 than the lateral force. In this study, for the same volume of material removed, the lateral
236 (F_x) and normal force (F_y) while cutting polycrystalline GaAs were about 70 nN and
237 110 nN respectively while the forces during cutting of the single crystal GaAs were of
238 the order of 90 nN and 130 nN, respectively.

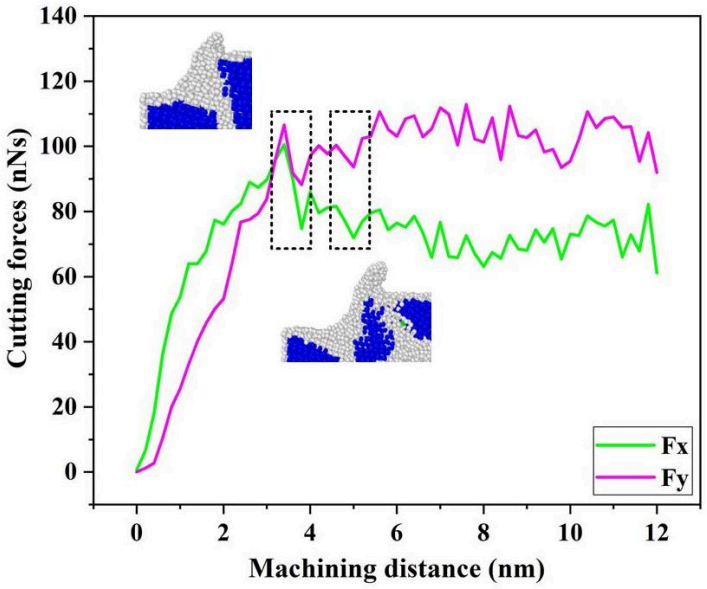

239

240 (a) Scratch forces during cutting of a polycrystalline GaAs

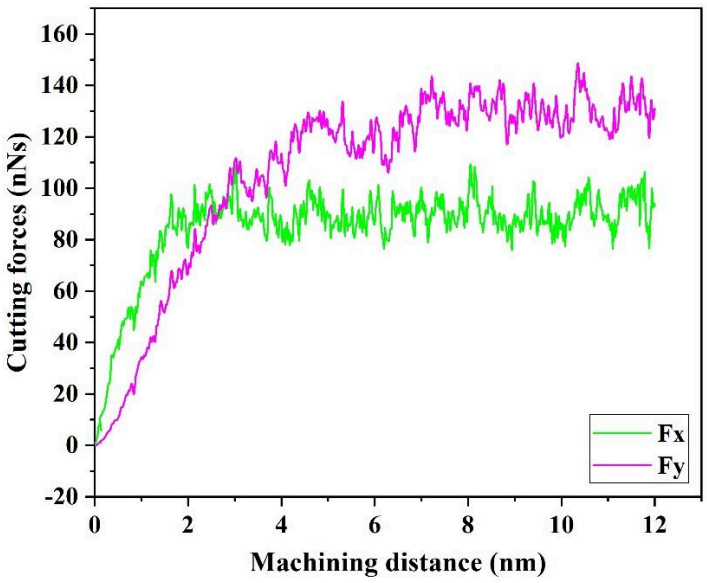

(b) Scratch forces during cutting of a single crystal GaAs

Fig. 8. Evolution of cutting forces i.e. lateral (F_x) and normal force (F_y) at a cutting velocity of 200 m/s and at depth of cut of 2 nm.

Furthermore, by comparing Fig. 8(a) and Fig. 8(b), it may be seen that the lateral (F_x) and normal force (F_y) smoothly undulated from crests to troughs during cutting of polycrystalline GaAs. The reason for this is that the cutting force drops as the grains started to slide along an easy slip direction and when the grain boundary paved the way for the plastic deformation causing the cutting energy to be mainly concentrated in the grain boundaries. Beyond a certain threshold, the grain boundary collapses releasing a burst of deformation energy which leads to wave troughs of the cutting force. Additional calculations of the specific cutting energy and friction coefficient (F_x/F_y) were also made. The specific cutting energy is defined as the work done by the tool in removing the unit volume of material and it can be calculated as [26].

$$Specific\ cutting\ energy\ = \frac{R}{b \times t} \quad (2)$$

where R refers to the resultant force $sqrt(F_x^2 + F_y^2)$ while b and t represents the width of cut and depth of cut, respectively.

As shown in Table 2, the resultant cutting force, specific cutting energy and kinetic coefficient of friction values for cutting polycrystalline substrate were seen to be lower in magnitude compared to cutting single crystal GaAs.

Table 2: Comparison of cutting results for single crystal GaAs and polycrystalline GaAs

Workpiece	F_x (nN)	F_y (nN)	F_r (nN)	Specific cutting energy (GPa)	Friction coefficient
Single crystal GaAs	91.56	127.35	156.85	27.46	0.719
Polycrystalline GaAs	70.21	103.40	124.98	21.88	0.679

The machining force results indicated that the polycrystalline GaAs was more machinable than the single crystal GaAs. This is due to the presence of grain boundaries which eases the ductile deformation of a polycrystalline substrate.

3.4 Influence of cutting depth and cutting speed

In this section, the influence of cutting depth and cutting speed on the cutting forces, sub-surface damage depth and the cutting temperature are reported. As shown in Fig. 9, both lateral (F_x) and normal forces (F_y) during cutting of the polycrystalline GaAs decreased with the increase of cutting speed or decreasing depth of cut. It was further observed that the normal force (F_y) continues to be higher than the lateral force (F_x) in all cases of scratching.

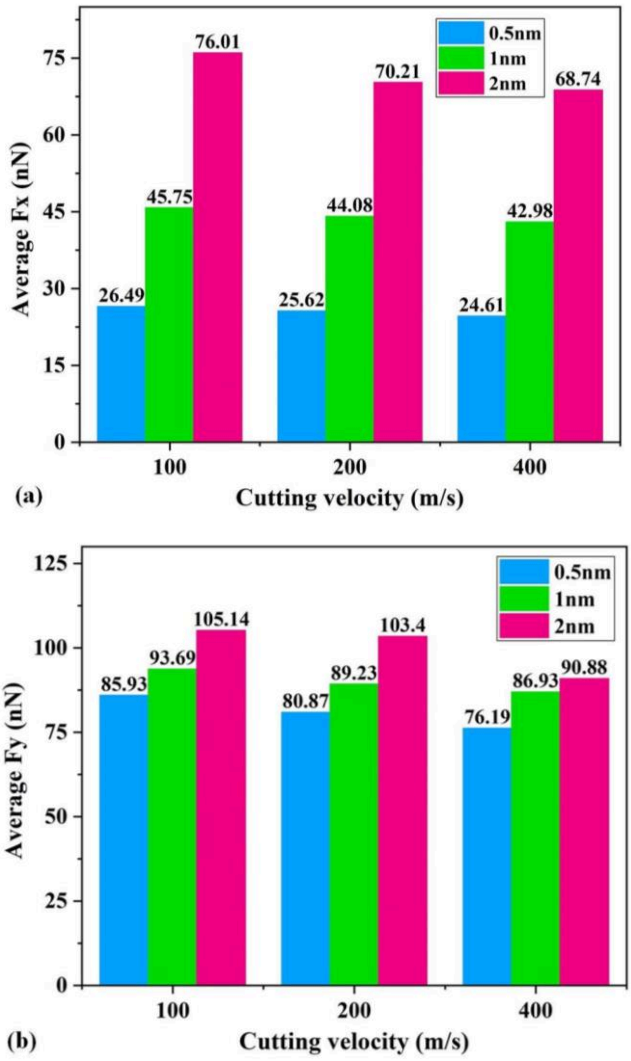

Fig. 9. The average value of the lateral (F_x) and normal forces (F_y) under different cutting velocities and depth of cut in cutting of polycrystalline GaAs.

Next, the sub-surface damage depth during cutting of polycrystalline GaAs was estimated as a function of different speeds and depth of cut which is shown in figure 10. It was seen that the damage depth reduces with the increasing cutting speed which indicates that high strain rate applied during cutting decreases the sub-surface damage. A maximum sub-surface damage reduction of 16.32% could be achieved while cutting at 400 m/s at a depth of cut of 2 nm in comparison to cutting at 100 m/s at the same

286 depth of cut.

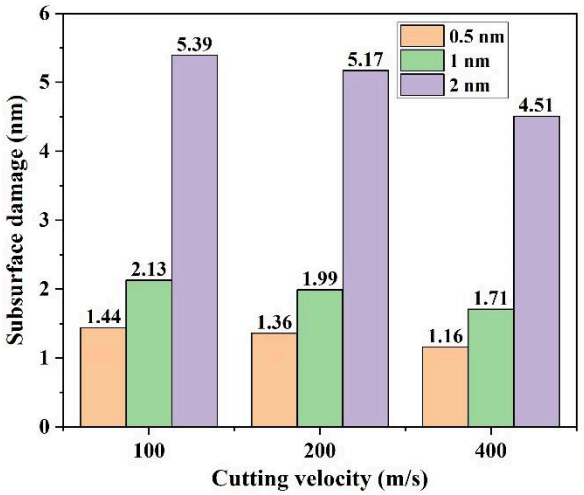

287

288 **Fig. 10.** Sub-surface damage depth at different cutting velocities and depth of cut

289 Finally, the temperature variation as a function of depth of cut and cutting speed was
290 estimated and shown in figure 11. Higher speed of cutting and higher depths of cutting
291 were both seen to accompany an increase in the cutting temperature in the plastic zone.
292 The combined information of the temperature and stresses acting in the cutting zone
293 could be used as a vital information to predict the microstructural changes in the cutting
294 zone and we shall expand on this aspect in our future work.

295

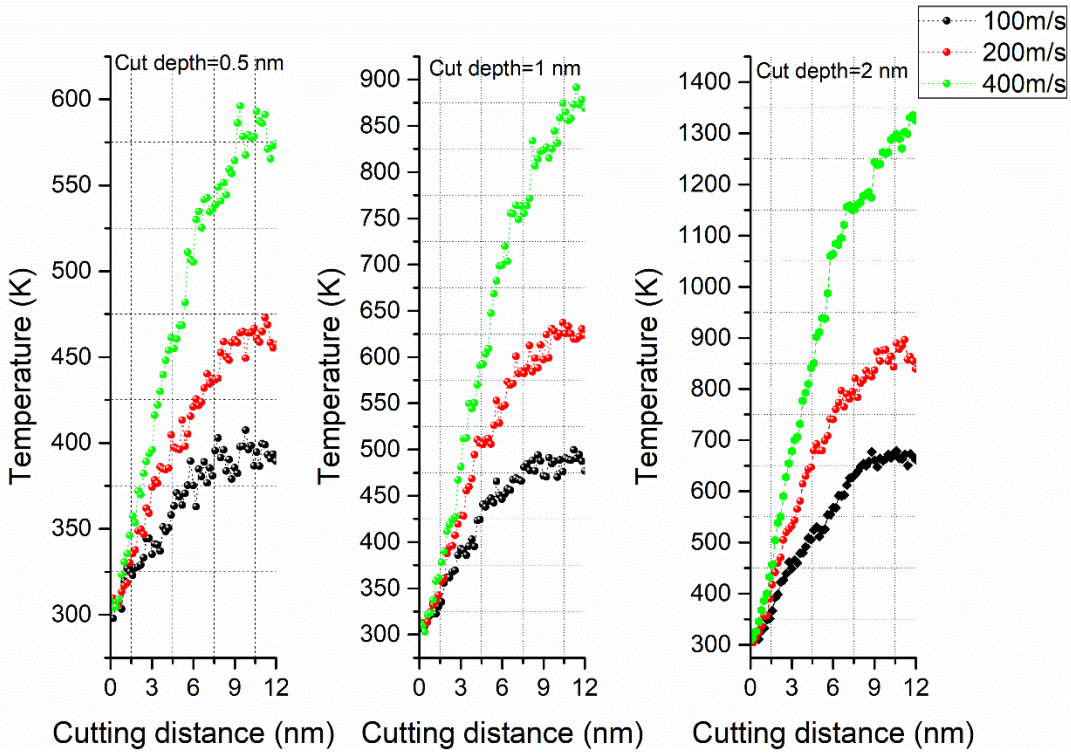

Fig. 11. Peak temperature variation at various scratch speeds and depth of cuts

4 Conclusions

In this work, the deformation mechanism of polycrystalline GaAs during nanoscratching was investigated by the MD simulations and benchmarked to single crystal GaAs. During the simulations, the scratch depth, speed of scratching (thus the applied strain rate) and microstructure of the workpiece (polycrystalline vs single crystal GaAs) were varied and output parameters such as the scratch forces (and specific cutting energy), kinetic coefficient of friction, cutting temperature, sub-surface damage and dislocation structures were extracted and analysed. In light of these extracted parameters and the analysis performed, the following conclusions can be drawn:

1. The presence of grain boundaries eases the deformation of the polycrystalline GaAs as opposed to single crystal GaAs. It was discovered that the grain boundaries can become the sites of dislocation nucleation and thus become the

311 weak links in a polycrystal as opposed to a single crystal which has no such
312 weaker links. The ease of plastic deformation of the grain boundaries compared
313 to the individual grains makes polycrystals more easily deformed than the single
314 crystals.

315 2. The cutting forces showed a unique cyclic wave crest to wave troughs transition
316 while cutting polycrystalline GaAs in contrast to the cutting of the single crystal
317 GaAs. This was attributable to the periodic arrest of the dislocations in the grain
318 boundaries followed by collapsed grain boundaries as a result of the continuous
319 tool penetration.

320 3. The friction coefficient and the specific cutting energy were found to be higher
321 for scratching single crystal GaAs than for polycrystalline GaAs and also the
322 normal scratch force achieves a higher magnitude over the lateral scratch force
323 once the scratching has achieved a steady state.

324 4. Scratch forces and the sub-surface damage were observed to reduce with an
325 increase in the scratch velocity and to increase with the increasing depth of
326 scratch. However, the cutting temperature increases with the increase in scratch
327 speed and the scratch depth.

328 5. Much like the typical diamond cubic lattice structures, the ½<110> was found
329 to be the main dislocation responsible for plasticity in GaAs which splits into
330 Shockley partials connected by an Internal Stacking Fault (ISF) leading to
331 dissociation of the parent dislocation in 1/6<121> and 1/6<211> type
332 dislocations.

Acknowledgement

The authors would like to thank EPSRC (EP/K018345/1, EP/T024844/1) and the Royal Society-NSFC international exchange programme (IEC\NSFC\181474) to provide financial support to this research. The authors also acknowledge the use of the EPSRC (EP/K000586/1) funded ARCHIE-WeSt High-Performance Computer at the University of Strathclyde for the MD simulation study.

SG is particularly thankful to the Research support provided by the UKRI via Grants No. EP/L016567/1, EP/S013652/1, EP/T001100/1, EP/S036180/1 and EP/T024607/1. Additionally, the support received from H2020 (Cost Actions (CA18125, CA18224, CA17136 and CA16235), Royal Academy of Engineering via Grants No. IAPP18-19\295, TSP1332 and EXPP2021\1\277 and Newton Fellowship award from the Royal Society (NIF\R1\191571) is also acknowledged. SG also accessed the Isambard Bristol, UK supercomputing service via Resource Allocation Panel (RAP) as well as ARCHER resources (Project e648).

Data statement

All data underpinning this publication are openly available from the University of Strathclyde Knowledge Base at https://doi.org/10.15129/ed05ea22-ab4c-4dd7-af36-4dfb91bd1cef.

Conflict of Interest: The authors declare that they have no conflict of interest.

References

[1] H. J. Ahn, W. Il Chang, S. M. Kim, B. J. Park, J. M. Yook, and Y. S. Eo, "28 GHz GaAs pHEMT MMICs and RF front-end module for 5G communication systems," *Microw. Opt. Technol. Lett.*, vol. 61, no. 4, pp. 878–882, 2019.

[2] J. H. Epple, K. L. Chang, C. F. Xu, G. W. Pickrell, K. Y. Cheng, and K. C. Hsieh, "Formation of highly conductive polycrystalline GaAs from annealed amorphous (Ga,As)," *J. Appl. Phys.*, vol. 93, no. 9, pp. 5331–5336, 2003.

[3] M. K. Sharma and D. P. Joshi, "Electrical conduction model for polycrystalline GaAs films," *J. Appl. Phys.*, vol. 102, no. 3, pp. 1–8, 2007.

[4] M. Imaizumi *et al.*, "Low-temperature growth of GaAs polycrystalline films on glass substrates for space solar cell application," *J. Cryst. Growth*, vol. 221, no. 1–4, pp. 688–692, 2000.

[5] J. C. Bourgoin, "Polycrystalline GaAs for large area imaging detectors," *Nucl. Instruments Methods Phys. Res. Sect. A Accel. Spectrometers, Detect. Assoc. Equip.*, vol. 466, no. 1, pp. 9–13, 2001.

[6] J. D. Song, W. J. Choi, J. I. Lee, J. M. Kim, K. S. Chang, and Y. T. Lee, "Optical and structural properties of InGaAs/InP double quantum wells grown by molecular beam epitaxy with polycrystalline GaAs and GaP decomposition sources," *Phys. E Low-Dimensional Syst. Nanostructures*, vol. 32, no. 1-2 SPEC. ISS., pp. 234–236, 2006.

[7] S. Z. Chavoshi, S. Xu, and S. Goel, "Addressing the discrepancy of finding the equilibrium melting point of silicon using molecular dynamics simulations,"

Proc. R. Soc. A Math. Phys. Eng. Sci., vol. 473, no. 2202, pp. 1–9, 2017.

[8] S. Goel, N. Haque Faisal, X. Luo, J. Yan, and A. Agrawal, "Nanoindentation of polysilicon and single crystal silicon: Molecular dynamics simulation and experimental validation," *J. Phys. D. Appl. Phys.*, vol. 47, no. 27, 2014.

[9] S. Goel, J. Yan, X. Luo, and A. Agrawal, "Incipient plasticity in 4H-SiC during quasistatic nanoindentation," *J. Mech. Behav. Biomed. Mater.*, vol. 34, pp. 330–337, 2014.

[10] S. Goel *et al.*, "Horizons of modern molecular dynamics simulation in digitalized solid freeform fabrication with advanced materials," *Mater. Today Chem.*, vol. 18, p. 100356, 2020.

[11] P. Hirel, "Atomsk: A tool for manipulating and converting atomic data files," *Comput. Phys. Commun.*, vol. 197, pp. 212–219, 2015.

[12] G. Voronoi, "Nouvelles applications des paramètres continus à la théorie des formes quadratiques. Deuxième mémoire. Recherches sur les parallélloèdres primitifs," *J. für die reine und Angew. Math.*, vol. 1908, no. 134, pp. 198–208, 2009.

[13] G. Lejeune Dirichlet, "Über die Reduction der positiven quadratischen Formen mit drei unbestimmten ganzen Zahlen.," *J. für die reine und Angew. Math.*, vol. 40, pp. 209–227, 1850.

[14] S. Nose, "A unified formulation of the constant temperature molecular-dynamics methods," *J. Chem. Phys.*, vol. 81, pp. 511–519, 1984.

[15] S. J. Plimpton, "Fast parallel algorithms for short range molecular dynamics,"

J. Comput. Phys., vol. 117, pp. 1–19, 1995.

[16] D. T. Infield *et al.*, "Main-chain mutagenesis reveals intrahelical coupling in an ion channel voltage-sensor," *Nat. Commun.*, vol. 9, no. 1, pp. 1–10, 2018.

[17] A. Stukowski, "Visualization and analysis of atomistic simulation data with OVITO-the Open Visualization Tool," *Model. Simul. Mater. Sci. Eng.*, vol. 18, no. 1, 2010.

[18] P. Erhart and K. Albe, "Analytical potential for atomistic simulations of silicon, carbon, and silicon carbide," *Phys. Rev. B - Condens. Matter Mater. Phys.*, vol. 71, no. 3, pp. 1–14, 2005.

[19] K. Albe, K. Nordlund, J. Nord, and A. Kuronen, "Modeling of compound semiconductors: Analytical bond-order potential for Ga, As, and GaAs," *Phys. Rev. B - Condens. Matter Mater. Phys.*, vol. 66, no. 3, pp. 352051–3520514, 2002.

[20] J. F. Ziegler, M. D. Ziegler, and J. P. Biersack, "SRIM - The stopping and range of ions in matter (2010)," *Nucl. Instruments Methods Phys. Res. Sect. B Beam Interact. with Mater. Atoms*, vol. 268, no. 11–12, pp. 1818–1823, 2010.

[21] E. Maras, O. Trushin, A. Stukowski, T. Ala-Nissila, and H. Jónsson, "Global transition path search for dislocation formation in Ge on Si(001)," *Comput. Phys. Commun.*, vol. 205, pp. 13–21, 2016.

[22] S. Goel and A. Stukowski, "Comment on 'incipient plasticity of diamond during nanoindentation' by C. Xu, C. Liu and H. Wang,: RSC Advances, 2017, 7, 36093," *RSC Adv.*, vol. 8, no. 10, pp. 5136–5137, 2018.

[23] S. Goel, X. Luo, P. Comley, R. L. Reuben, and A. Cox, "Brittle-ductile transition during diamond turning of single crystal silicon carbide," *Int. J. Mach. Tools Manuf.*, vol. 65, pp. 15–21, 2013.

[24] Z. Li and R. C. Picu, "Shuffle-glide dislocation transformation in Si," *J. Appl. Phys.*, vol. 113, no. 8, pp. 1–7, 2013.

[25] S. H. He, B. B. He, K. Y. Zhu, and M. X. Huang, "Evolution of dislocation density in bainitic steel: Modeling and experiments," *Acta Mater.*, vol. 149, pp. 46–56, 2018.

[26] S. Goel, "The current understanding on the diamond machining of silicon carbide," *J. Phys. D. Appl. Phys.*, vol. 47, no. 24, 2014.